NANO · MICRO
small

Supporting Information

for *Small*, DOI 10.1002/smll.202305831

Local Heat Dissipation and Elasticity of Suspended Silicon Nanowires Revealed by Dual Scanning Electron and Thermal Microscopies

Jose M. Sojo-Gordillo, Gerard Gadea-Diez, David Renahy, Marc Salleras, Carolina Duque-Sierra, Pascal Vincent, Luis Fonseca, Pierre-Olivier Chapuis*, Alex Morata*, Séverine Gomès* and Albert Tarancón**

Local heat dissipation and elasticity of suspended silicon nanowires revealed by dual scanning electron and thermal microscopies – Supplementary Information

Finite Element Model of the Pd/nitride thin film cantilever

The conversion of measured tip resistance change in thermal conductances described by Equation 2 of the core manuscript relies on the use of a Finite Element Model (FEM) of the tip as highlighted in Figure 2a. Geometrical dimensions were determined from the probe analysis performed in Figure S4 and fixed constants. As depicted in the right lower corner of Figure 1c, because the bulk material was over-etched at the base of the nitride cantilever in the used tip, a fraction of the membrane needs to be simulated as well in order to account for this additional thermal resistance. The only geometrical free parameters were the gold and platinum thicknesses which were used to adjust each of the tip electrical resistances, namely Pd, Au, and NiCr thin films. In order to avoid many computationally expensive simulations with the FEM code, a first approximation of those values could be carried out using the approaches described by Puyoo *et al.*,[20] Pic *et al.*[49] and Guen *et al.*[50] It consists in solving the following system of equations:

$$R_{tip} = R_{Pd} + R_{Au} + R_{NiCr} \tag{S1}$$

$$R_{tip}\,\alpha_{tip} = R_{Pd}\,\alpha_{Pd} + R_{Au}\,\alpha_{Au} + R_{NiCr}\,\alpha_{NiCr}, \tag{S2}$$

where the tip global electrical resistance R_{tip} and its temperature coefficient of resistance α_{tip} can be determined from the data of Figure S5a. Complementary, as described in Table S1, R_{NiCr} was directly measured using microprobes, and the different material temperature coefficients of resistance α_i are taken from the literature.[20,51] The solution of this equation yields a first approximation of the electrical resistance of each part. Then, making use of the dependence of $R_i(h_i)$ obtained by the FEM model, they can be converted in thickness (h_i) values. The thin-film electrical conductivities were obtained from literature,[52,53] whereas thermal conductivities of metals were estimated using Wiedemann–Franz law. In these assumptions, a constant ratio between bulk and thin-film conductivities is expected both for electrical and thermal terms as both magnitudes are directly proportional in metals:

$$\kappa_{film} = \kappa_{bulk} \frac{\sigma_{film}}{\sigma_{bulk}}. \tag{S3}$$

Finally, the FEM is fine-tuned by varying the thermal conductivity of the nitride thin film – which is known to significantly vary with the deposition process from 0.5 up to 8 W/m·K[54] – and by minor changes in the metal thin films thicknesses in order to precisely match both self-heating and furnace curve simultaneously (Figure S5). Once calibrated, a sample conductance is added to the apex of the probe in the FEM. As Figure S6 illustrates, this boundary condition allows to estimate the effects for high contact conductances on the temperature distribution of the probe. Ultimately, the variation in tip temperature caused by the presence of a highly conductive sample marks the upper limit of conductance measurable under the assumption of constant tip temperature operation.[55]

Mechanical uncertainty analysis

Systematic errors in the force curve are derived from the calibration process. They can be condensed in the coefficient $\partial F/\partial V$ used to convert the interferometer voltage readout into the force applied. It basically depends on two sources, the one associated with the tip elastic constant $K_{probe} = \partial F/\partial z$ determination and the error derived from the fit of $\partial V/\partial z$:

$$\epsilon_{\partial F/\partial V} = \sqrt{\left(\epsilon_{K_{probe}}\right)^2 + \left(\epsilon_{\partial V/\partial z}\right)^2} \tag{S4}$$

An overall systematic error is estimated in 5.6% for the force measurement. However, the stochastic variation of the measurement, i.e. the reproducibility of the steps carried out over the same point, also contributes to the uncertainty of the measurement. In those cases, an average standard variation of the global elastic constant K_{eq} is estimated to be 16.1%. Hence, the error in the estimation of the NW elastic constant is derived from the systematic error of $\partial F/\partial V$ and the average variation of K_{eq}, resulting in a total error of 17.0%.

$$\epsilon_{K_{NW}} = \sqrt{\left(\epsilon_{\partial F/\partial V}\right)^2 + \left(\sigma_{K_{eq}}\right)^2} \tag{S5}$$

Thermal uncertainty analysis

A noticeable variation was found in the electrical resistance with null dissipated power $R_{P=0}$ during the experiment. Figure S5b compares the curves taken before and after the experiment. This is likely due to drift in the electrical contact of the tip during the experiment, as the overall dependence with the dissipated power does not change. Thus, these changes are attributed to the power-independent contribution of the tip resistance and do not affect the tip calibration sensitivity α_{tip}. The effect on the calculated conductance is corrected over the experimental data by computing the dissipated heat of each curve with the resistance measured at that precise moment. Since all conductance curves are offset with their absolute value, changes in their base value produced by the tip-sample interactions can be compared safely between each data-set.

Systematic errors of the measurements can be condensed in the coefficient α_{tip} related to the slope of the inset of Figure 2 though $\alpha_{tip} = R_{tip}^{-1}\partial R/\partial T_{tip}$. This parameter is used to translate the measured electrical changes in the tip electrical resistance into changes of the thermal conductance. It can be described as:

$$\epsilon_G = \epsilon_{\alpha_{tip}} = \sqrt{\left(\epsilon_{\partial R_{tip}/\partial P}\right)^2 + \left(\epsilon_{\partial R_{tip}/\partial T}\right)^2 + \left(\epsilon_{\alpha_{Au}R_{Au}}\right)^2 + \left(\epsilon_{R_{NiCr}}\right)^2} \tag{S6}$$

where ϵ_i denotes the relative error of the variable i. The first two error terms are related to the fittings of the calibration data used ($\partial R_{tip}/\partial P$ and $\partial R_{tip}/\partial T$). Typically the uncertainty in R_{NiCr} arises from the variability of the fabrication process compared to the tip specifications. However, the values used in this work were experimentally measured and therefore the error is negligible. Then, the error of the $\alpha_{Au}R_{Au}$ product arises from the differences between reported values and the tuned values used to adjust the model to the calibration data. A high interdependence between this value and the thicknesses of the Pd and Au films was found, making this factor one of the main sources of error for the estimation of α_{tip}. Hence, the overall systematic error is estimated in 10.7%

Additionally, a source of error arises from the approximation of a constant temperature rise at the tip apex θ_{tip} during the contact event. The approximation assumes that the newly created heat pathway at the apex of the tip G_c is negligible compared to the cantilever conductance. Figure S6 illustrates the variation of θ_{tip} obtained from the FEM presented in Figure 2 upon an increasing contact conductance. For the range of G_c studied in this work, a fluctuation of 1.6% is expected.

Another source of error is related to the stochastic variation of the measurement, i.e. the reproducibility of the steps carried out over the same point. This uncertainty strongly depends on the exact point of contact and thus the contact area. An average standard variation of ΔG of 2.7% has been estimated for the case of steps over the bulk, and of 2.8% for the steps over the NWs. This results in an overall uncertainty of 3.9%. Figure 2 differentiates this error from the systematic ones described for α_{tip}.

Finally, the error in the estimation of the thermal conductivity is derived from the measurement of the actual NW diameter ϕ (5.3%), the systematic error derived from α_{tip} (3.9%), and the average variation of ΔG both on the NW and on the bulk (used to calculate the contact resistance). Hence the estimation in the thermal conductivity results in a total error of 12.5%.

$$\epsilon_{\kappa_{NW}} = \sqrt{(2\epsilon_{\phi})^2 \left(\epsilon_{\alpha_{tip}}\right)^2 + (\epsilon_{\theta})^2 + \left(\sigma_{\Delta G}^{NW}\right)^2 + \left(\sigma_{\Delta G}^{Bulk}\right)^2} \tag{S7}$$

Supplementary figures

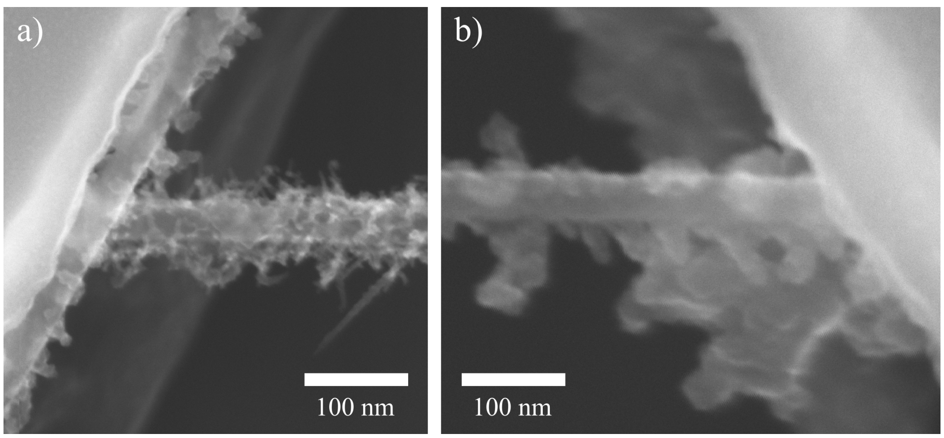

Figure S1: SEM images of the NW diameter at both ends. The geometric-mean diameter ($\phi = \sqrt{\phi_1 \phi_2}$) was used.

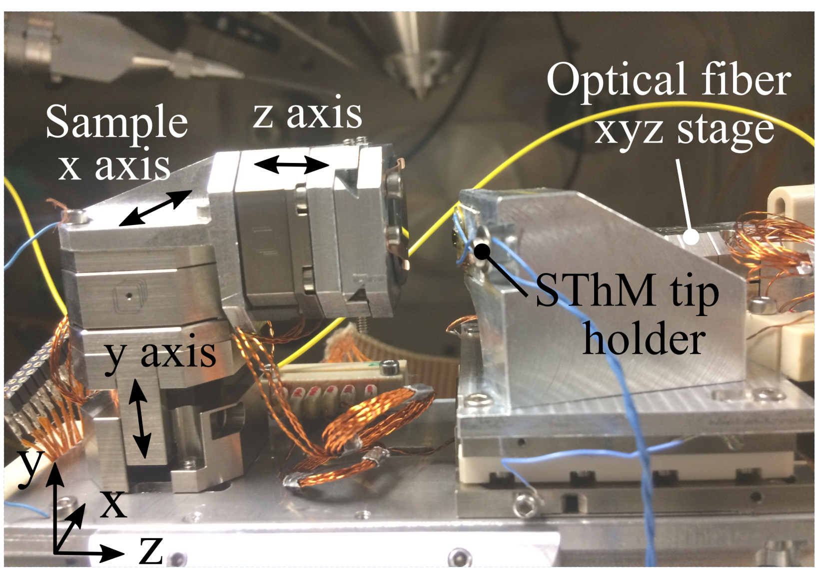

Figure S2: Image of the device inserted in the SEM chamber.

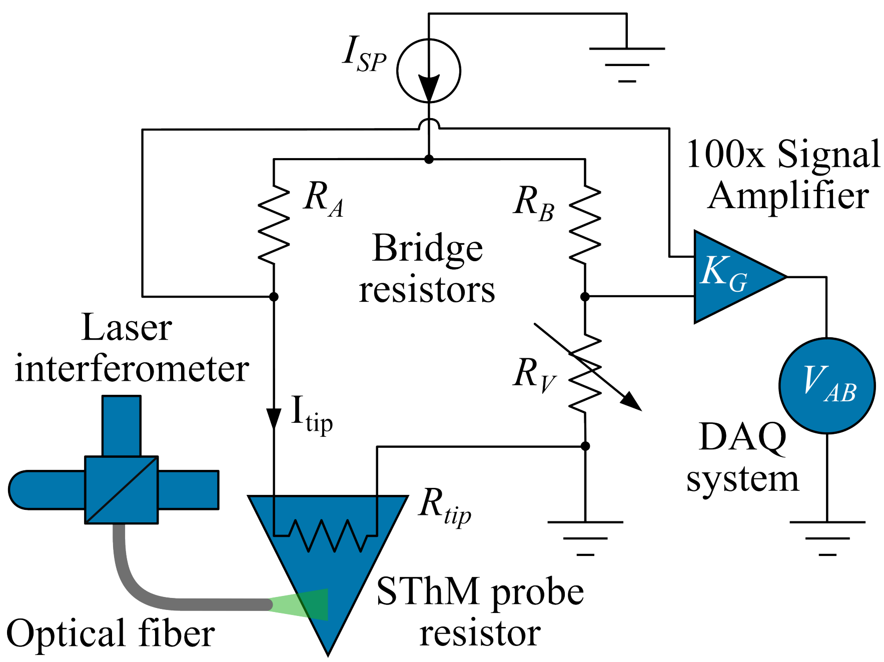

Figure S3: Diagram of the electrical and optical connection of the setup, showing the Wheatstone bridge and the interferometer used to determine tip conductance and the cantilever deflection respectively. A signal amplifier with a gain factor K_G was before reading the values with the data acquisition system (DAQ).

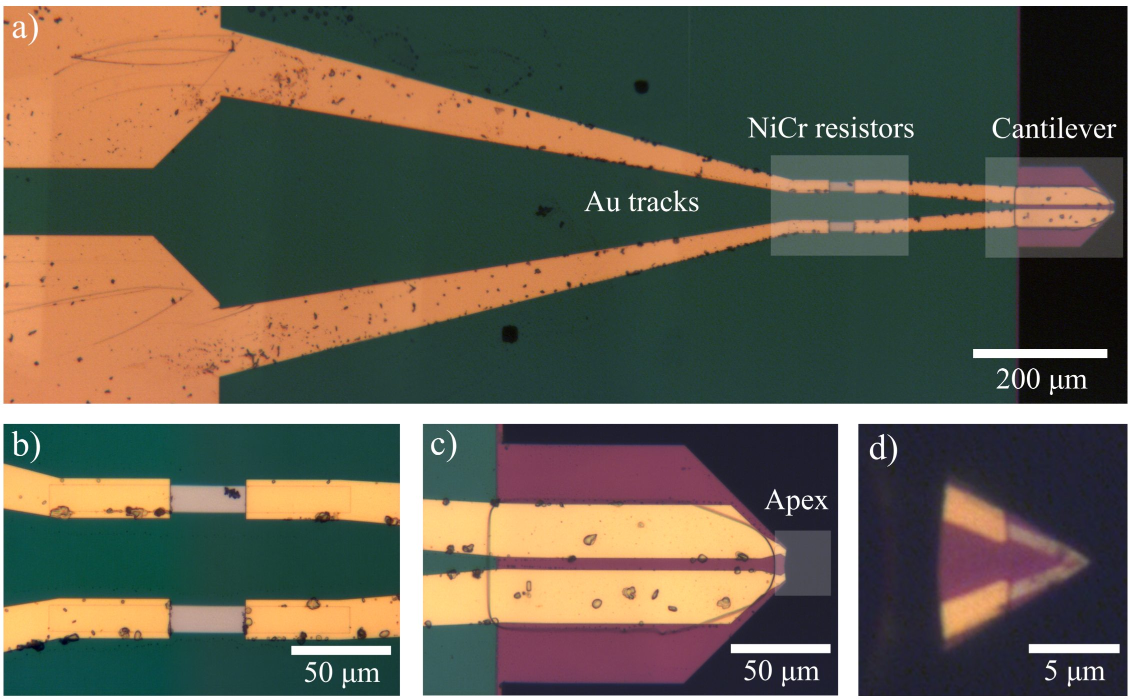

Figure S4: Optical images of the used 2nd generation Pd/nitride thin film SThM probe manufactured by KNT at different magnifications. a) Overview showing the Au tracks from the pads (left) to the cantilever. b) NiCr thin film resistance located on the bulk. c) Cantilever. d) Tip apex including the Pd resistor (grey). The image was taken tilting the tip by 45°.

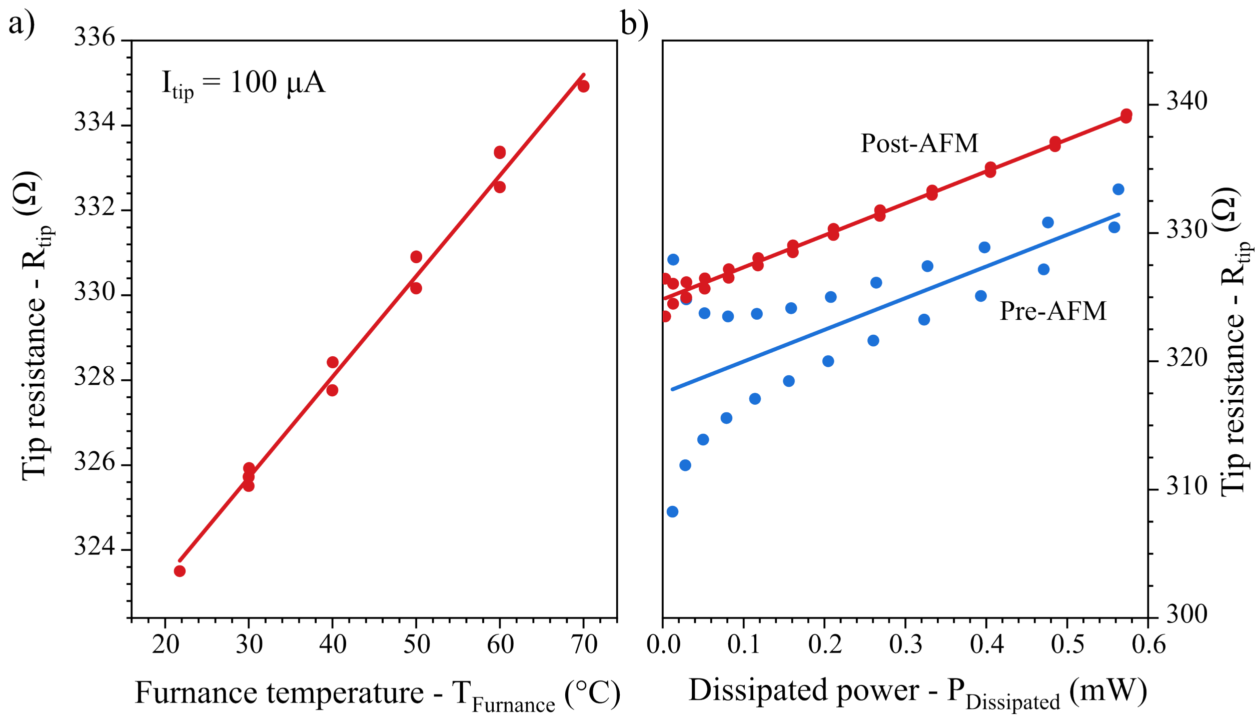

Figure S5: a) Tip resistance as a function of temperature. The value was measured using low current (100 µA) to prevent self-heating effects. b) Tip resistance as a function of the dissipated power applied to the tip. The curve was measured before and after the SThM measurements.

Table S1: Summary of the FEM parameters used to simulate the Pd/nitride thin film probe.

	Palladium		Gold		Nickel-Chromide		Nitride	
Parameter	Value	Source	Value	Source	Value	Source	Value	Source
σ (S/cm)	1.25×10^5	Ref. 52	3.1×10^4	Ref. 16	10^5	Ref. 53	-	-
α ($10^{-3}\,\mathrm{K}^{-1}$)	1.20	Ref. 16,51	2.00	Ref. 20,51	0.24	Ref. 20,51	-	-
κ (W/m·K)	23.2	Eq. S3	89.7	Eq. S3	-	-	4.3	FEM Fit
t (nm)	50	Ref. 56	140	Ref. 56	-	-	450	SEM
R_0 (Ω)	92.2	Eq. S1 and S2	45.0	Eq. S1 and S2	185.9	Exp.*	-	-

All values given at 300 K.

* Experimentally measured with microprobes.

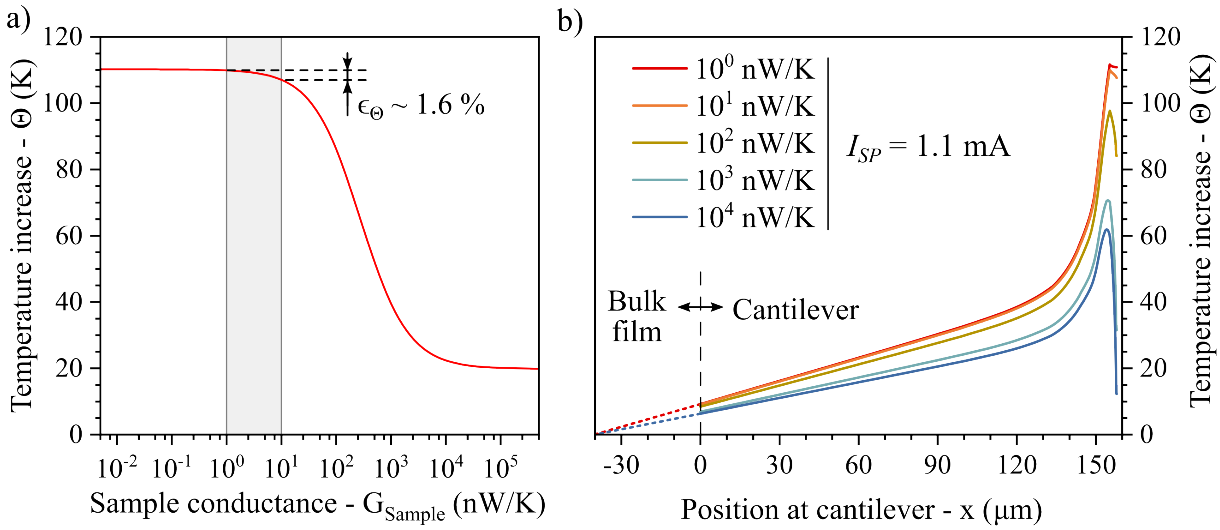

Figure S6: a) SThM probe temperature increase at the apex θ as a function of the contact conductance G_C i.e. the total sample conductance including the contact resistance when heated with a constant current of 1.1 mA (the same used during the experiments). The range of values measured in this work are highlighted with the shaded area ($1 - 10\,\mathrm{nW/K}$). b) Cantilever temperature profiles analogous to Figure 2 for contact conductances ranging from 1 nW/K to 10 µW/K.

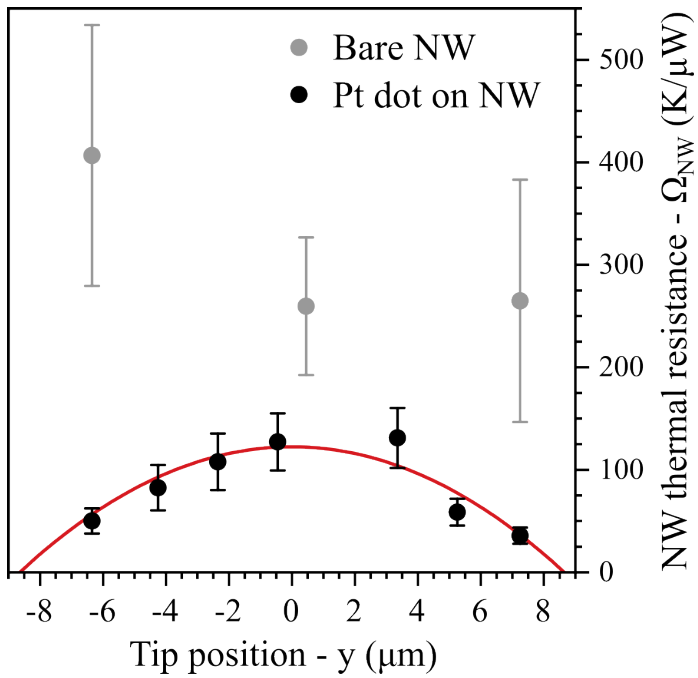

Figure S7: Nanowire local thermal resistance as a function of the tip position along the NW over Pt nanodots (black) or over bare rough surface of the NW (grey). Each point is the average of all the approach curves performed over the same point.